

VORTEX IN CELL METHOD FOR EXTERIOR PROBLEMS

HENRYK KUDELA
TOMASZ KOZŁOWSKI

*Wroclaw University of Technology, Department of Numerical Flow Modelling, Wroclaw, Poland
e-mail: tomasz.kozlowski@pwr.wroc.pl; henryk.kudela@pwr.wroc.pl*

The "vortex in cell" method was used to model the flow past a solid body. Problems connected with flows past a body belong to the category of exterior problems. The main difficulty here is to establish the boundary condition far from the body, to solve equations of motion on the numerical mesh. The mesh requires a limited calculation area and the boundary condition far from the body. A method of obtaining the accurate boundary condition in such flows was presented. Testing calculations were performed for the flow past a cylinder for a wide range of Reynolds numbers. The flow past an ellipse was also performed. A good agreement with experimental results and calculations of other researchers was obtained.

Key words: vortex method, flow past cylinder, external problem

1. Introduction

Vortex particle methods have obtained already the state of maturity and precision that one can compare them to the accuracy and efficiency of the classic method like the finite difference method or spectral method (Cottet et al, 2000, 2002). The importance of the vortex particle method lies in the possibility of analysing more easily and directly the vorticity field due to the fact that in computations particles that carry information about the vorticity field are used. The vorticity is the key to understanding many hydrodynamic phenomena (Kudela and Machela, 2007). An attractive feature of the method is also elimination of difficulties connected with modelling of the inertial terms of Navier-Stokes equations. In the present work, the Vortex-In-Cell (VIC) method was used to determine the flow past a solid body in an infinite domain. Such a problem belongs to the category of exterior problems. The difficulty in

numerical modelling of such a problem is related to the establishment of the boundary condition far from the body. The mesh requires a finite calculation area, and the boundary condition far from the body is needed. In direct vortex methods, which use the Biot-Savart law to calculate the velocity field, the condition at infinity is satisfied automatically. However, direct vortex methods are very time consuming. The VIC method is hundreds times faster than the direct method (Cottet and Poncet, 2003). The VIC method retains the important features of particle methods that solve the convective part of fluid motion. The grid is used to compute the velocity by solution of the Poisson equation for stream function and vorticity. To manage the far field boundary condition, we used the method described in Anderson and Reider (1996), Wang (1999). That method takes advantage of the fact that the domain of non-zero vorticity around the solid body is limited to the domain around the obstacle. In the far distance from the body, where the vorticity is zero, the asymptotic properties of the Laplace equation and its solution represented by Fourier series is used. It enables determination of the proper far field boundary condition. In order to use the fast direct algorithm for the solution of the Poisson equation on a uniform grid we applied the conformal mapping. We tested the VIC method for the flow over a circular cylinder and elongated shape of an ellipse. We were especially interested in the ability of the VIC method for reproduction of very fine vortex structures near the solid body.

2. Vortex particle method and conformal mapping

Two-dimensional equations of an incompressible viscous fluid transformed to the Helmholtz equation for stream function and vorticity are

$$\omega_t + u\omega_x + v\omega_y = \nu\Delta\omega \quad \Delta\Psi = -\omega \quad (2.1)$$

The velocity of the fluid is determined as

$$u = \partial_y\Psi \quad v = -\partial_x\Psi \quad (2.2)$$

The subscripts denote partial differentiation with respect to the variable that appears in the subscript. Equations (2.1) need to be completed with initial conditions for the vorticity field $\omega(x, y, 0) = \omega_0 = \text{rot}(u_0)$, where u_0 denotes the initial velocity field $u(x, y, 0) = u_0$ and non-slip boundary condition on the solid wall for the velocity.

Zeroing of the normal velocity component is obtained by setting $\Psi = \text{const}$ on the wall. Zeroing of the tangential velocity is satisfied by introducing a proper portion of vorticity that ensures $\mathbf{u} \cdot \mathbf{s} = 0$ where \mathbf{s} is a unit tangential vector.

To transform the non-rectangular physical region (x, y -variables) to the rectangular one (ξ, η), we used the conformal mapping. In the new variables (ξ, η), equations (2.1) take form (Graham, 1988)

$$\omega_t + u\omega_\xi + v\omega_\eta = \frac{\nu}{J}\Delta\omega \quad \Delta\Psi = -J\omega \tag{2.3}$$

where J denotes Jacobian of the conformal transformation

$$J = \det \begin{vmatrix} x_\xi & x_\eta \\ y_\xi & y_\eta \end{vmatrix} \tag{2.4}$$

and the velocities are expressed by the formulas

$$u = \frac{1}{J}\partial_\eta\Psi \quad v = -\frac{1}{J}\partial_\xi\Psi \tag{2.5}$$

In the VIC method, the continuous vorticity field is approximated with a discrete particles distribution. The flow region is covered with the numerical grid $h = \Delta\eta = \Delta\xi$, (ih, jh) , $(i = 1, 2, \dots, n_\xi, j = 1, 2, \dots, n_\eta)$. In the grid nodes, the particles with Γ_j circulation are placed

$$\Gamma_j = \int_A \omega \, d\xi d\eta \tag{2.6}$$

where $A = h^2$, and

$$\omega(\xi, \eta) = \sum_p \Gamma_p \delta(\xi - \xi_p) \delta(\eta - \eta_p) \tag{2.7}$$

The viscous splitting algorithm was used for solution of (2.3) and (2.5). Firstly, the inviscid fluid equation was solved

$$\omega_t + u\omega_\xi + v\omega_\eta = 0 \tag{2.8}$$

From (2.3)₁ it stems that the vorticity is constant along the trajectory of fluid particles. According to the Helmholtz theorem (Wu *et al.*, 2005), vortex particles are moving like material fluid particles. Differential equation (2.8) is replaced by the infinite set of ordinary equations

$$\begin{aligned} \frac{d\xi}{dt} &= u & \frac{d\eta}{dt} &= v \\ \xi(0, \alpha_1) &= \alpha_1 & \eta(0, \alpha_2) &= \alpha_2 \end{aligned} \tag{2.9}$$

where $\alpha = (\alpha_1, \alpha_2)$ means Lagrangian coordinates of fluid particles. The infinite set of differential equations (2.9) is replaced by a finite one. The number of particles is equal to the number of grid nodes. The Lagrangian parameter α takes in each time step the value $\alpha_i, \alpha_j = (\xi_i, \eta_j)$. The finite set of equations (2.9) was solved by the Runge-Kutta method of the fourth order. The velocity field was obtained by solving Poisson equation (2.3)₂ on the numerical grid and making use of (2.5). The velocities of particles that are found between the grid nodes were calculated by the interpolation formula

$$u(\xi_p, \eta_p) = \sum_j l_j(\xi_p, \eta_p) u_j \quad (2.10)$$

where l_j denotes the two-dimensional bilinear interpolation Lagrange base.

The viscosity was taken into account by solving the diffusion equation

$$\omega_t = \frac{\nu}{J} \Delta \omega \quad \omega(\xi, \eta, 0) = \omega_0 \quad \omega|_{wall} = \omega_s \quad (2.11)$$

where ω_s was calculated on the basis of Poisson equation (2.3)₂. Taking into account the non-slip condition $u = 0$, it gives the vorticity on the wall $\omega = -\Psi_{\eta\eta}/J$. The value of this vorticity was calculated by the Briley formula (Weinan and Liu, 1996)

$$\omega_{(0,j)_s} = -\frac{1}{J} \frac{108\Psi_{1,j} - 27\Psi_{2,j} + 4\Psi_{3,j}}{18h^2} + O(h^4) \quad (2.12)$$

where h denotes the grid step, index 0 refers to the wall and index i ($i = 1, 2, 3$), to the distance ih from the wall.

In order to solve the diffusion equation on the grid, after displacement of particles according to equation (2.9), it was necessary to pass the vorticity from the particles to the grid nodes. In each time step, redistribution of masses of vortex particles onto neighbouring grid nodes was performed (Fig. 1), according to the formula

$$\omega_{ij} = \frac{1}{h^2} \sum_p \Gamma_p \varphi_h(\xi) \varphi_h(\eta) \quad (2.13)$$

where

$$\varphi_h(\xi) = \varphi\left(\frac{\xi - \xi_i}{h}\right) \quad \varphi_h(\eta) = \varphi\left(\frac{\eta - \eta_j}{h}\right)$$

Indexes p, i, j refer to vortex particles and grid nodes, respectively, and $\varphi(\cdot)$ is the kernel of the interpolation function. The fourth order interpolation kernel,

known in the literature as the M4, was used (Becerra-Sagredo, 2003; Cottet and Koumoutsakos, 2000)

$$\varphi(x) = \begin{cases} 1 - \frac{5}{2}x^2 + \frac{3}{2}|x|^3 & \text{for } |x| < 1 \\ \frac{1}{2}(2 - |x|)^2(1 - |x|) & \text{for } 1 \leq |x| \leq 2 \\ 0 & \text{for } |x| > 2 \end{cases} \quad (2.14)$$

For particles near the wall, one-sided interpolation functions were used (2.15) derived according to the algorithm presented in Becerra-Sagredo (2003)

$$\varphi(x) = \begin{cases} 1 + \frac{1}{2}x^2 - \frac{3}{2}|x| & \text{for } j = 0, |x| \leq 1 \\ -x^2 + 2|x| & \text{for } j = 1, |x| \leq 1 \\ \frac{1}{2}x^2 - \frac{1}{2}|x| & \text{for } j = 2, |x| \leq 1 \end{cases} \quad (2.15)$$

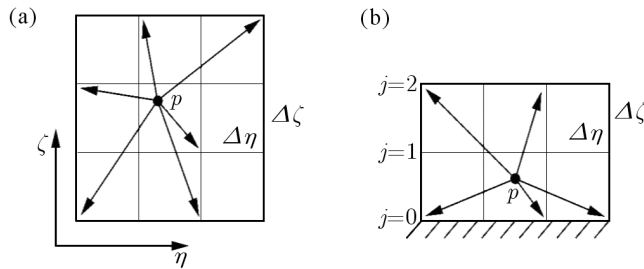


Fig. 1. Redistribution of particle masses onto neighboring grid nodes, (a) for particles inside the computational domain (at least one cell from the wall), (b) for the particles in the vicinity of the wall

The interpolation of particle masses onto grid nodes has fundamental meaning for precision of the VIC method. Both interpolation kernels conserve three first moments (Cottet and Koumoutsakos, 2000)

$$\sum_p x_p^\alpha \varphi\left(\frac{x_p - x}{h}\right) = x^\alpha \quad \alpha = 0, 1, 2 \quad (2.16)$$

Diffusion equation (2.11)₁ was solved on the numerical grid with the alternating direction implicit scheme (Thomas, 1995)

$$\omega^{n+\frac{1}{2}} = \omega^n + \frac{\Delta t}{2J} \nu (\Lambda_{\xi\xi} \omega^n + \Lambda_{\eta\eta} \omega^{n+\frac{1}{2}}) \quad (2.17)$$

$$\omega^{n+1} = \omega^{n+\frac{1}{2}} + \frac{\Delta t}{2J} \nu (\Lambda_{\xi\xi} \omega^{n+1} + \Lambda_{\eta\eta} \omega^{n+\frac{1}{2}})$$

where Δ means the three point finite difference quotient that approximates the Laplace operator with respect to the variable that was put in the lower index. The solution of the diffusion equation ends the calculations in the n -th time step of the vortex particles method. The full computational algorithm can be summarised as follows:

- The whole computational domain is covered by the numerical grid. In every grid node, the vortex particle is placed with the circulation given by Eq. (2.6).
- The Poisson equation for stream function and vorticity is solved, Eq. (2.3)₂, the velocities on the grid nodes are computed, Eq. (2.5).
- The equation of motion of the inviscid fluid is solved by displacements of the particles, Eq. (2.9).
- After displacements of the particles, the redistribution process of particle circulation to the grid nodes takes place, Eqs. (2.13)-(2.15).
- The proper amount of vorticity that is needed to fulfil the non-slip condition on the wall is calculated, Eq. (2.12).
- The diffusion equation is solved, Eq. (2.11)₁, with scheme (2.17).

This ends one time step.

3. Far field boundary condition for the Poisson equation

Here we present a method how to obtain the accurate boundary condition for the Poisson equation for the exterior problem. We follow the description that was given by Wang (1999). Due to the fact that we used the finite difference method for the solution of the Poisson equation, our realisation is a bit different than in Wang (1999).

Let us write the boundary value problem for the Poisson equation in an unbounded area

$$\Delta\Psi = -\omega \quad \Psi(R_1, \theta) = z(\theta) \quad (3.1)$$

where $z(\theta)$ is a known function. In the problem of the flow past a solid body, the vorticity ω is different from zero, in some limited area around the body. This area can be enclosed in a finite ring with radius $r = a$, Fig. 2. The condition for $\Psi(R_2, \theta)$ is unknown. In the area $r > a$, vorticity equals zero. Since equation (3.1)₁ had been solved by the finite difference method, the calculation area was enclosed in the ring $R_1 < r < R_2$. In our approach,

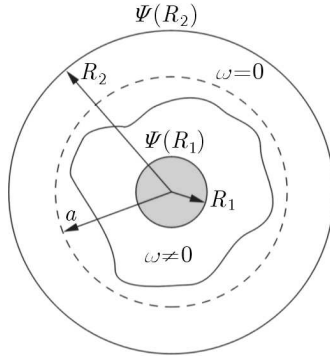


Fig. 2. Finite computational domain for grid Poisson solver $R_1 < r < R_2$ and distribution of vorticity around the cylinder

in order to determine the accurate boundary condition on the external radius $r = R_2$, the Poisson equation was solved twice. First, a trial solution was determined Ψ_{trial} with a fictitious boundary condition on a large radius e.g. $\Psi_{trial}(R_2) = \Gamma \ln(R_2)$, where Γ means any constants

$$\begin{aligned} \Delta \Psi_{trial} &= -\omega & (3.2) \\ \Psi_{trial}(R_1) &= z(\theta) & \Psi_{trial}(R_2) = \Gamma \ln(R_2) \end{aligned}$$

Let Ψ denote the exact solution to problem (3.1)₁, and Ψ_1 the difference between the trial and exact solutions, $\Psi_1 = \Psi_{trial} - \Psi$. The error Ψ_1 is a harmonic function as it is a solution to the Laplace equation. The accurate solution is also harmonic in the area without vorticity, $r > a$. The error Ψ_1 has in the ring $R_1 < r < R_2$ a Fourier series representation (Farlow, 1993; Wang, 1999)

$$\Psi_1(r, \theta) = a_n \ln(r) + \sum_{n \geq 1} \left(b_n + \frac{c_n}{r^n} \right) e^{in\theta} \tag{3.3}$$

where a_n, b_n, c_n are Fourier coefficients which will be determined from boundary conditions. Outside the domain where $\omega(r, \theta) \equiv 0$, it is for $r > a$, $\Psi(r, \theta)$ can be presented as (Farlow, 1993; Wang, 1999)

$$\Psi(r, \theta) = \Gamma \ln(r) + \sum_{n \geq 1} \frac{d_n}{r^n} e^{in\theta} \tag{3.4}$$

The Fourier coefficients b_n, c_n, d_n in equations (3.3) and (3.4) can be determined on the basis of the following boundary conditions

$$\begin{aligned}\Psi(R_1, \theta) &= 0 \\ \Psi_{trial}(R_2, \theta) &= \Psi(R_2, \theta) + \Psi_1(R_2, \theta) \\ \frac{\partial \Psi_{trial}}{\partial r}(R_2, \theta) &= \frac{\partial \Psi}{\partial r}(R_2, \theta) + \frac{\partial \Psi_1}{\partial r}(R_2, \theta)\end{aligned}\quad (3.5)$$

Conditions (3.5)_{2,3} express the continuity of Ψ and its first derivative with respect to r for the radius $r = R_2$. The derivative of the trial solution $\partial \Psi_r(R_2, \theta) = g(\theta)$ was calculated by the one-sided finite difference formula of the fourth order

$$\begin{aligned}g(\theta) &= \frac{1}{12h} [3\Psi_{trial}(r_{n-4}, \theta) - 16\Psi_{trial}(r_{n-3}, \theta) + 36\Psi_{trial}(r_{n-2}, \theta) + \\ &\quad - 48\Psi_{trial}(r_{n-1}, \theta) + 25\Psi_{trial}(r_n, \theta)] + O(h^4)\end{aligned}\quad (3.6)$$

Having the values of $g(\theta)$, we expanded this expression into the Fourier series

$$g(\theta) = f_0(R_2) + \sum_{n>1} f_n(R_2)e^{in\theta}\quad (3.7)$$

Series (3.7) approximates the left side of formula (3.5)₃. The right side of (3.5)₃ was obtained by differentiating series (3.3) and (3.4). Using equations (3.5) and (3.7) the Fourier coefficients a_n, b_n, c_n, d_n can be expressed as

$$\begin{aligned}a_n &= 0 & b_n &= \frac{f_n(R_2)}{2nR_2^{n-1}} \\ c_n &= -b_nR_1^{2n} & d_n &= b_n(R_1^{2n} - R_2^{2n})\end{aligned}\quad (3.8)$$

One can see from (3.8), that coefficients b_n, c_n, d_n are expressed by the known coefficient f_n . Using the trial solution with the fictitious boundary condition $\Psi_{trial}(R_2, \theta)$, the accurate value of the boundary condition can be determined

$$\Psi(R_2, \theta) = \Psi_{trial}(R_2, \theta) - \sum_{n \geq 1} \frac{f_n(R_2)}{2n} R_2 \left(1 - \frac{R_1^{2n}}{R_2^{2n}}\right) e^{in\theta}\quad (3.9)$$

The procedure for getting of the proper boundary value for $r = R_2$ goes as follows:

- First, the Poisson equation was solved using the finite difference method with the fictitious boundary condition on the larger radius $\Psi_{trial}(R_2, \theta)$
- The derivative of the solution obtained on the external radius $g(\theta)$ was determined numerically and expanded into the Fourier series

- The correction of the boundary condition was made according to equation (3.9)
- The Poisson equation was solved again with the accurate condition on the radius R_2 .

The Poisson equation was solved by a fast direct algorithm of $O(h^4)$ order of accuracy. The order of the correction method was the same as the order of the used solver for the Poisson equation.

4. Flow past a circular cylinder

At first, we checked the above procedure for the far field boundary condition and the vortex particle ability to reproduce very fine vortex structures. The calculations were carried out for a well documented flow over a circular cylinder. The following conformal transformation was used

$$x + iy = e^{r+i\theta} \quad (4.1)$$

The Jacobian of the transformation is presented with the following formula

$$J = e^{2r} \quad (4.2)$$

The physical flow region in Fig. 3a was transformed onto the rectangle, Fig. 3b.

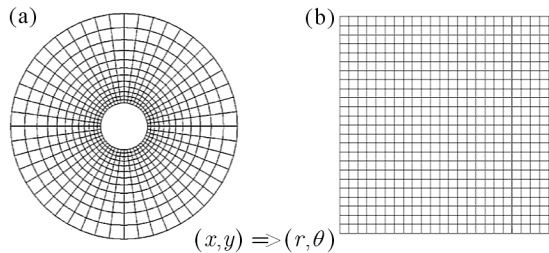


Fig. 3. Transformation of the physical domain by conformal mapping (4.1) for the flow past a cylinder: (a) grid in the physical domain, (b) rectangular grid in the computational domain

The calculations were carried out on a regular numerical mesh $h = \Delta\theta = \Delta r$, (ih, jh) , $(i = 1, 2, \dots, n_r, j = 1, 2, \dots, n_\theta)$.

The Poisson equation for stream function and vorticity was solved in the transformed coordinates (r, θ) which corresponded, according to (4.1),

to $R_1 = 1$, $R_2 = e^\pi$ in the computational domain. The Poisson equation was solved with the following boundary conditions

$$\Delta\Psi = -\frac{\omega}{J} \quad \Psi(R_1, \theta) = 0 \quad \Psi(R_2, \theta) = \Psi_c \quad (4.3)$$

where Ψ_c denotes the corrected stream function value as it was described in the previous section. At the first step it was assumed that $\Psi_\infty = U_\infty R_2 \cos \theta$, $U_\infty = 1$. When treating the problem with a sudden impulsive flow over the cylinder, one encounters the transition problem which has consequences in oscillatory solutions in the initial time steps. To eliminate the transition, a smooth start was performed. In the first calculation step, the vorticity equaled zero and it a potential solution was assumed. The velocity at infinity of the flow, changed linearly from zero to U_∞ , in the time interval $[0, t_s]$. Then we restarted the calculation using the obtained solution for $t = t_s$ as the new initial condition for the vorticity field. In each time step that followed, on the external radius a correction of the boundary condition Ψ_c was made as described in Section 3.

Calculations were carried out for a wide range of Reynolds numbers $Re = U_\infty 2R_1/\nu$. The parameter of the numerical grid, time steps and t_s are presented in Table 1. For comparison, the drag force and drag coefficient were determined on the surface of the cylinder (Anderson and Reider, 1996)

$$F_D = b\mu \int_0^{2\pi} \left(\omega - R \frac{\partial \omega}{\partial r} \right) R \sin \theta \, d\theta \quad (4.4)$$

$$C_D = \frac{F_D}{\rho u_\infty^2 R b}$$

where μ is the dynamic coefficient of fluid viscosity, $\mu = \rho\nu$, ρ is density of the fluid, b denotes the unit length of the cylinder and R denotes its radius. We assumed $R = 1$, $\rho = 1$.

Table 1. Grid parameters and time steps for the flow past a circular cylinder

Re	n_r	n_θ	Δt	t_s
550	256	512	0.01 s	0.2 s
3000	512	1024	0.005 s	0.3 s
9500	2048	4096	0.002 s	0.4 s

A characteristic feature of the flow past the cylinder is appearance of recirculation bubbles behind the cylinder for $Re < 50$ (Bourd and Coutanceau,

1980; Van Dake, 1982). For Reynolds numbers $Re > 50$, the bubbles are no longer stationary and alternately separate from the cylinder wall creating Karman's vortex street, Fig. 5 (Van Dake, 1982). In Fig. 4 it a comparison of the numerical streamline distribution for the Reynolds number $Re = 3000$ and $t = 5$ with the experimental one is shown (Van Dake, 1982). The ability of reproduction of a fine vortex structure on the cylinder is clearly visible. The numerical results for $Re = 9500$ is presented in Fig. 6. Qualitatively, a very good agreement was obtained with the visualization data that were published in Van Dake (1982).

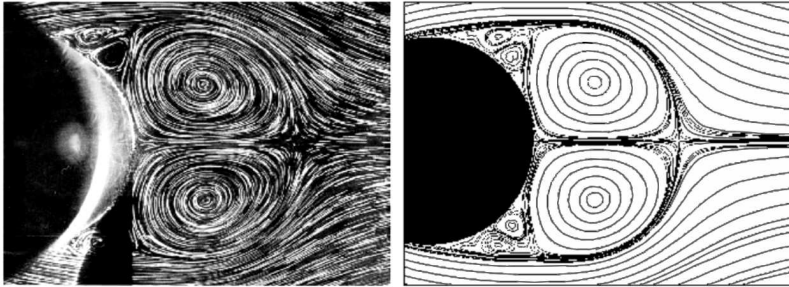


Fig. 4. Comparison of the streamline distribution for the flow past the cylinder, $Re = 3000$, $t = 5s$, experiment (Van Dake, 1982) (left) and numerical computations (right)



Fig. 5. Exemplary picture of the vortex Karman street, $Re = 550$, $t = 100s$

In Fig. 7 a comparison of the calculated drag coefficient with the results of Koumoutsakos and Leonard (1995) is presented. Some discrepancies are observed for times $t < 1$. They can be related to the problem how one managed the transition at the beginning of calculations (Anderson and Reider, 1996; Koumoutsakos and Leonard, 1995). In the present work, the initial condition for vorticity was obtained by smooth start. The noted differences at the beginning did not influence the results significantly in later time steps. For the Reynolds number $Re = 9500$ the correct reproduction of vortex structures in the vicinity of the wall requires a very dense numerical mesh (see Table 1).

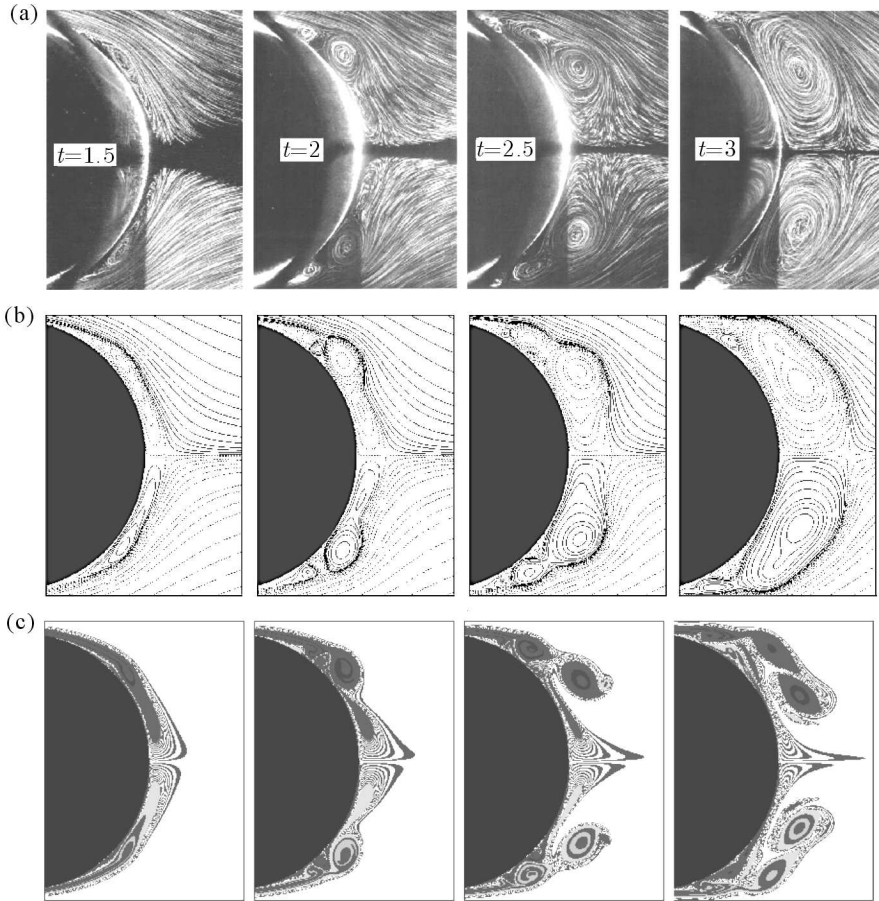


Fig. 6. Comparison of evolution of streamlines with the experimental data. Evolution of vorticity for $Re = 9500$; (a) experimental data (Van Dake, 1982), (b) streamlines from computation, (c) computed isolines of vorticity

5. Flow past an elliptic cylinder

The next test was dedicated to more complicated shape of the solid body. We investigated the flow past a thin ellipse perpendicular to the flow direction. The calculations were carried out in elliptic coordinates, which were transformed onto a regular Cartesian mesh using conformal transformations (Fig. 8a)

$$x + iy = \cosh(\xi + i\eta) \quad (5.1)$$

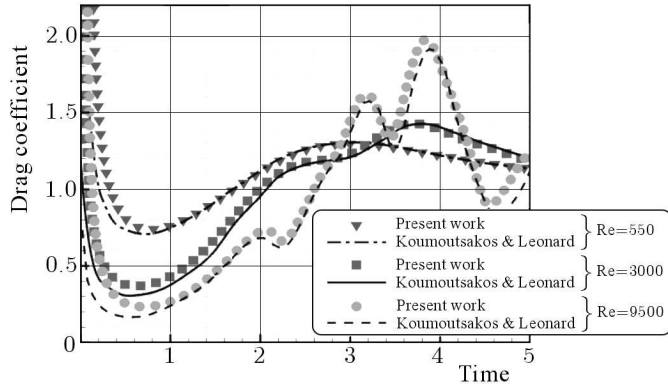


Fig. 7. Comparison of time evolution of the drag coefficient with the results by Koumoutsakos and Leonard (1995)

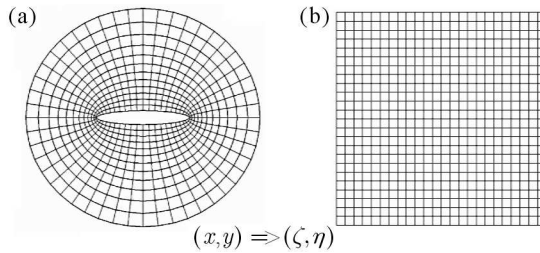


Fig. 8. (a) Elliptical grid in the physical domain, (b) rectangular grid in the computational domain after transformation

The Jacobian of this mapping is

$$J = \cosh^2 \xi - \cos^2 \eta \tag{5.2}$$

The calculations were carried out for the following parameters: ellipse thickness $e = 0.25$, ellipse length $L = 2$, Reynolds number $Re = 500$ and 10000 . On the sharp ends of the ellipse, significant vorticity is generated. A dense grid in this region (Fig. 8a), allows one to reproduce flow phenomena generated in this area, however a small time step is required, $\Delta t = 0.0005$. For low Reynolds numbers, behind the ellipse, vortex structures are generated (Fig. 9), which after some time become separated from the wall, forming Karman’s vortex street.

At high Reynolds numbers, along the line that forms the main vortex structure, smaller secondary vortex structures appear (Figs. 10, 11). Numerical calculations carried out in Koumoutsakos and Shields (1996), Wang *et al.* (1999) qualitatively reflect the phenomenon discussed. It was found by Wang

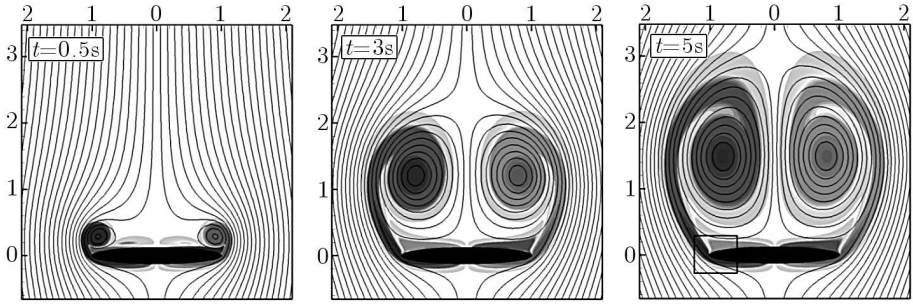


Fig. 9. Vorticity and streamlines for the flow past an ellipse, $Re = 500$

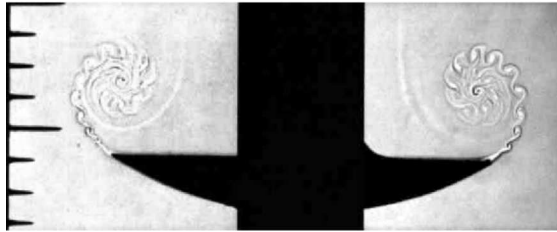


Fig. 10. Visualization of growth of vortices on the accelerated plate Van Dake (1982)

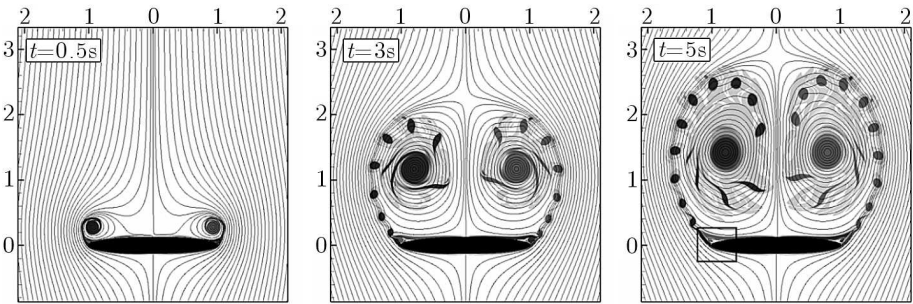


Fig. 11. Vorticity and streamlines for the flow past the ellipse, $Re = 10000$.
Secondary vortices along the primary vortex is visible

et al. (1999) that the frequency of the small secondary vortex is controlled by the vortex which appears near the sharp edge of the ellipse (corner vortex), Fig. 12b. After sudden start, the corner vortex reaches a quasi-stationary state. The calculations were carried out for the same parameters as in Wang *et al.* (1999). The vorticity generated at the end of the ellipse very well agrees with the results of Wang *et al.* (1999). In Fig. 10, the experimental visualization of Van Dake (1982) was presented. The similarity of the visualization data and numerical results is visible.

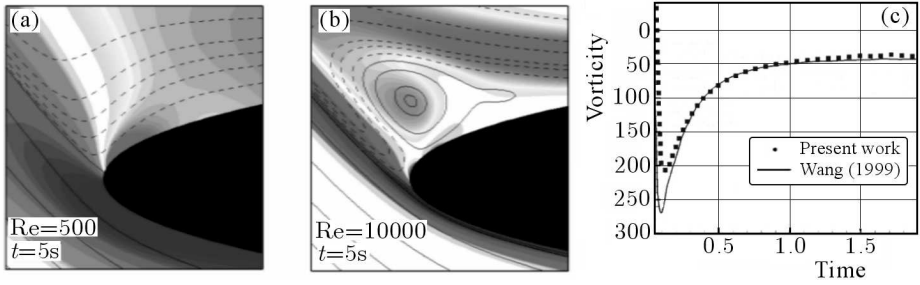


Fig. 12. Image of the vorticity field and streamlines in the vicinity of the wall (a) $Re = 500$, (b) $Re = 10000$, (c) comparison of the vorticity distribution on the sharp end of the ellipse with the results by Wang *et al.* (1999)

6. Remarks on realisation of boundary conditions

The generated portion of the vorticity on the solid boundary to satisfy the no-slip condition on the wall must fulfill some constraints. Let us denote the whole vorticity in the domain as

$$\Omega(t) = \int_D \omega(x, y, t) \, dx dy \tag{6.1}$$

Taking into account that the divergence of $\nabla \cdot (\omega \mathbf{u}) = \nabla \omega \cdot \mathbf{u}$, ($\nabla \cdot \mathbf{u} = 0$, $\nabla = (\partial_x, \partial_y)$), where \mathbf{n} is the unit normal vector, then integrating Helmholtz equation (2.1)₁ by sides, and using the Gauss divergence theorem, one obtains

$$\frac{d}{dt} \Omega(t) + \int_{\partial D} (\omega \mathbf{u} \cdot \mathbf{n} - \nu \nabla \omega \cdot \mathbf{n}) \, dC = 0 \tag{6.2}$$

where $C = \partial D$ is the boundary of the domain. On the solid boundary we have $\mathbf{u} \cdot \mathbf{n} = 0$. So it stems from equation (6.2) that

$$\frac{d}{dt} \Omega(t) = \nu \int_{\partial D} \frac{\partial \omega}{\partial \mathbf{n}} \, dC \tag{6.3}$$

It is clear that global vorticity (6.1) in the domain can only change due to the flux of vorticity through the boundary. But the right-hand side of equation (6.3) should be zero to satisfy the single-value property of pressure. Going around the boundary of the profile, we have

$$\nu \int_{\partial D} \frac{\partial \omega}{\partial \mathbf{n}} \, dC = \int_{\partial D} \frac{\partial p}{\partial \mathbf{s}} \, dC \tag{6.4}$$

where \mathbf{s} means the tangent unit vector. So global vorticity (6.1) in the domain should not change, and in our case should be zero. The changes of the global vorticity in the domain during calculations for the flow over the cylinder was presented in Fig. 13. One can see that the maximum fluctuations of the total value of vorticity depend on Reynolds number. The maximum fluctuations is on the level $\pm 2 \cdot 10^{-10}$, for the Reynolds number $\text{Re} = 9500$. Taking into account the comparison with the experimental and numerical data presented in the previous Section, it seems to be acceptable. For an acceptable outcome of the non-slip boundary conditions at greater Reynolds numbers, the grid near the boundary should be finer.

In literature (Koumoutsakos *et al.*, 1994; Cottet and Koumoutsakos, 2000; Kudela and Malecha, 2007), instead of the values of vorticity generated on the wall to satisfy the no-slip condition, one can meet the generation of proper values of the flux of the vorticity. This flux of vorticity is determined by the formula (Koumoutsakos *et al.*, 1994)

$$\frac{\partial \omega}{\partial \mathbf{n}} = -\frac{\gamma}{\nu \Delta t} \quad (6.5)$$

where $\gamma = \llbracket u_s \rrbracket$ means the intensity of the vortex sheet along the solid boundary that is equal to the jump of the velocity from zero to the spuriously induced velocity on the solid boundary. We checked both methods and obtained nearly the same results.

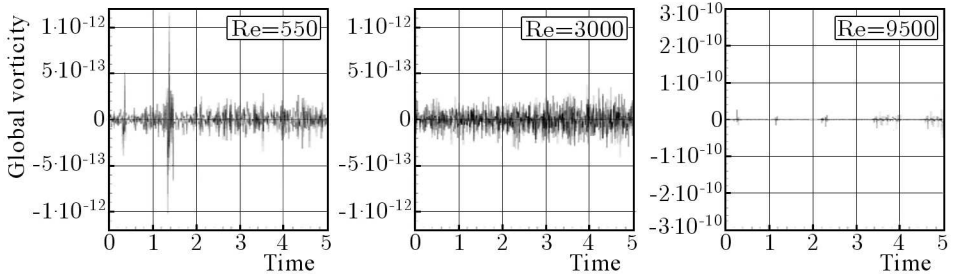


Fig. 13. Changes of global vorticity for the calculated flow over the cylinder

7. Conclusion

From the numerical results that are presented in the paper, one can conclude that the VIC method with conformal mapping and the algorithm for determination of the far field boundary condition is effective and accurate. The VIC

method with generation of vorticity on the boundary to satisfy the no-slip condition is also accurate and able to reproduce a very fine vortex structure that arises at the solid boundary. The vortex particle methods are especially well suited for the problem governed by the vorticity and vortex structures. That situation takes place when we study flows over solid bodies. Due to the fundamental meaning of vorticity in fluid mechanics, the importance of the vortex particle method in numerical fluid mechanics arises as well.

References

1. ANDERSON CH.R., REIDER M.B., 1996, A High order explicit method for the computation of flow about a circular cylinder, *J. Comp. Phys.*, **125**
2. BECERRA-SAGREDO J.T., 2003, Moment conserving cardinal splines interpolation of compact support for arbitrarily spaced data, *Research Report No. 10*, Zurich, Switzerland
3. BOUARD R., COUTANCEAU M., 1980, The early stage of development of the wake behind an impulsively started cylinder for $40 < \text{Re} < 104$, *J. Fluid Mech.*, **101**, 583
4. COTTET G.H., KOUMOUTSAKOS P., 2000, *Vortex Methods Theory and Practice*, Cambridge University Press, Cambridge
5. COTTET G.H., MICHAUX B., OSSIA S., VANDERLINDEN G., 2002, Comparison of spectral and vortex methods in three dimensional incompressible flows, *J. Comp. Phys.*, **175**
6. COTTET G.H., OULD-SALIHI M.L., EL HAMRAOUI M., 2000, Blending finite-difference and vortex methods for incompressible flow computations, *J. Sci. Comput.*, **22**, 5
7. COTTET G.H., PONCET P., 2003, Advances in direct numerical simulations of 3D wall-bounded flows by vortex-in-cell methods, *J. Comp. Phys.*, **193**
8. FARLOW J.S., 1993, *Partial Differential Equations for Scientists and Engineers*, Dover Publications, New York
9. GRAHAM J.M.R., 1988, Computation of viscous separated flows using a particle method, *Numerical Methods in Fluid Dynamics III*, Oxford
10. KOUMOUTSAKOS P., LEONARD A., 1995, High-resolution simulations of flow around an impulsively started cylinder using vortex method, *J. Fluid Mech.*, **296**
11. KOUMOUTSAKOS P., LEONARD A., PEPIN F., 1994, Boundary conditions for Viscous Vortex Methods, *J. Comp. Phys.*, **113**

12. KOUMOUTSAKOS P., SHIELDS D., 1996, Simulations of the viscous flows normal to an impulsively started and uniformly accelerated flat plate, *J. Fluid Mech.*, **328**, 177
13. KUDELA H., 1999, Application of the Vortex-In-Cell method for the simulation of two-dimensional viscous flow, *Task Quarterly*, **3**, 3
14. KUDELA H., MALECHA Z., 2007, Investigation of unsteady vorticity layer eruption induced by vortex patch using vortex particles method, *J. Theoret. and Appl. Mech.*, **45**, 785
15. THOMAS J.W., 1995, *Numerical Partial Differential Equations: Finite Difference Methods*, Springer
16. VAN DAKE M., 1982, *An Album of Fluid Motion*, Stanford, California
17. WANG Z.J., 1999, Efficient implementation of the exact numerical far field boundary condition for Poisson equation on an infinite domain, *J. Comp. Phys.*, **153**, 666
18. WANG Z.J., LIU J.-G., CHILDRESS S., 1999, Connection between corner vortices and shear layer instability in flow past an ellipse, *Physics of Fluids*, **11**, 9
19. WEINAN E., LIU J.-G., 1996, Vorticity boundary conditions and related issues for finite difference schemes, *J. Comp. Phys.*, **124**, 66
20. WU J.Z., MA H.Y., ZHOU M.D., 2005, *Vorticity and Vortex Dynamics*, Springer

Metoda cząstek wirowych dla zagadnień zewnętrznych

Streszczenie

Przedstawiono wyniki obliczeń dla zagadnienia zewnętrznego opływu ciała. Do obliczeń zastosowano metodę cząstek wirowych typu „wir w komórce”. Rzeczywisty obszar przepływu transformowano używając odwzorowania konforemnego. Opisano sposób wyznaczania zewnętrznego warunku brzegowego daleko od ciała, wykorzystując asymptotyczne własności rozwiązania równania Laplace’a. Wyniki numeryczne przedstawiono dla opływu walca w szerokim przedziale liczb Reynoldsa ($550 \leq \text{Re} \leq 9500$) oraz cienkiej elipsy. Obliczenia porównano z danymi eksperymentalnymi i wynikami numerycznymi innych badaczy, uzyskując bardzo dobrą zgodność.

Manuscript received July 18, 2008; accepted for print April 8, 2009